Comparison between a generalized Newtonian model and a network-type multiscale model for hemodynamic behavior in the aortic arch: Validation with 4D MRI data for a case study

Marine Menut, Loic Boussel, Xavier Escriva, Benyebka Bou-Saïd, Hélène Walter-Le Berre, Yann Marchesse, Antoine Millon, Nellie Della Schiava, Patrick Lermusiaux, John Tichy

Comparison between a generalized Newtonian model and a network-type multiscale model for hemodynamic behavior in the aortic arch: Validation with 4D MRI data for a case study

Marine Menut [a,*], Loïc Boussel [b,c], Xavier Escriva [d], Benyebka Bou-Saïd [a], Hélène Walter-Le Berre [a], Yann Marchesse [e], Antoine Millon [f,g], Nellie Della Schiava [f], Patrick Lermusiaux [f,g], John Tichy [h]

[a] *Université de Lyon, CNRS INSA-Lyon, LaMCoS, UMR5259, F-69621, France*
[b] *Department of Radiology, Hôpital de la Croix-Rousse, Hospices Civils de Lyon, Lyon, France*
[c] *CREATIS, CNRS UMR 5220-INSERM U1206 – Université de Lyon, Lyon, France*
[d] *Université Claude Bernard Lyon 1, LMFA, Ecole Centrale de Lyon, INSA Lyon, CNRS UMR5509, France*
[e] *Université de Lyon, ECAM Lyon, INSA Lyon, LabECAM, F-69005 Lyon, France*
[f] *Service de chirurgie vasculaire, Hospices Civils de Lyon, France*
[g] *Université Claude Bernard Lyon 1, France*
[h] *Rensselaer Polytechnic Institute, Department of Mechanical, Aerospace, and Nuclear Engineering, Troy, NY 12180-3590, USA*

Blood is a complex fluid in which the presence of the various constituents leads to significant changes in its rheological properties. Thus, an appropriate non-Newtonian model is advisable; and we choose a Modified version of the rheological model of Phan-Thien and Tanner (MPTT). The different parameters of this model, derived from the rheology of polymers, allow characterization of the non-Newtonian nat-ure of blood, taking into account the behavior of red blood cells in plasma. Using the MPTT model that we implemented in the open access software OpenFOAM, numerical simulations have been performed on blood flow in the thoracic aorta for a healthy patient. We started from a patient-specific model which was constructed from medical images. Exiting flow boundary conditions have been developped, based on a 3-element Windkessel model to approximate physiological conditions. The parameters of the Windkessel model were calibrated with *in vivo* measurements of flow rate and pressure. The influence of the selected viscosity of red blood cells on the flow and wall shear stress (WSS) was investigated. Results obtained from this model were compared to those of the Newtonian model, and to those of a gen-eralized Newtonian model, as well as to *in vivo* dynamic data from 4D MRI during a cardiac cycle. Upon evaluating the results, the MPTT model shows better agreement with the MRI data during the systolic and diastolic phases than the Newtonian or generalized Newtonian model, which confirms our interest in using a complex viscoelastic model.

1. Introduction

The role of hemodynamics in the formation of aneurysms, especially in the cane-shaped aortic arch, is well accepted in the literature. Various authors (Boussel et al., 2009; Pedersen et al., 1999; Pedersen et al., 1993) have shown the existence of preferential sites for the formation of aneurysms and found that a weak and oscillating Wall Shear Stress (WSS) promotes the development of an aneurysm by its impact on the shape and structure of the endothelial cells. The improvement of medical imaging techniques (Hope et al., 2010; Markl et al., 2010; Sigovan et al., 2011; Millon et al., 2014; Sigovan et al., 2015) provides more accurate information on the rheological behavior of blood. In addition to ultrasonic imaging, which is often hampered by organs covering the arterial vessels, the radiologist now has phase-contrast magnetic resonance sequences that can be applied to most arterial sites, which allow the *in vivo* determination of the velocity field. This type of work is particularly interesting in comparing rheological fluid models and validating their assumptions in numerical simulations. However, difficulties persist among previous authors (Taylor et al., 1998; Moore et al., 1999; Löhner et al., 2003), particularly with

* Corresponding author at: INSA Lyon – LaMCoS, 27 bis Avenue Jean Capelle, Bâtiment Sophie Germain, 69621 Villeurbanne cedex, France.
E-mail address: marine.menut@insa-lyon.fr (M. Menut).

regard to boundary conditions, biological material parameters, and blood rheology.

Previous studies (Rayz et al., 2008; Boussel et al., 2009; Rayz et al., 2010; Rayz et al., 2015) use numerical models based on medical imaging to simulate flow in aneurysms. Computational Fluid Dynamics (CFD) patient-specific simulations performed for measured flow conditions are compared with *in vivo* measurements of 4D MRI. These simulations can help determine which surgical option is likely to reduce the flow in the aneurysm while preserving overall blood flow. This methodology has been successfully applied to surgical procedures and planning such as the design and optimization of aortic endovascular stents (Figueroa et al., 2009; Gallo et al., 2016).

In these numerical simulations, blood rheology, by its shear-thinning and thixotropic nature, is strongly influenced by the unsteady nature of shear stress in the flow. Several hemodynamic flow studies were performed on realistic thoracic aorta geometries which confirmed the disturbances and helical character of the flow observed in this area (Dwyer et al., 2002; Morris et al., 2005; Liu et al., 2009; Nayak et al., 2015).

It appears that the rheological aspect of the blood has a significant impact on the arterial wall response. The purpose of this investigation is thus to use a numerical approach based on the Modified Phan-Thien and Tanner model in order to study its capability to predict correctly both pressure and velocity fields. This article is organized as follow: first, rheological models are presented, then the numerical approach to simulate blood flow in a patient-specific case study is detailed. Results are finally compared with the ones reached experimentally (i.e. *in vivo*).

2. Rheological models

Blood is a complex fluid in which the presence of its various constituents leads to significant changes in rheological properties. The anatomy of the thoracic aorta gives the flow a complex morphology that includes areas of recirculation and helical motion (Hope et al., 2010; Stankovic et al., 2014).

For a complete description of hemodynamic phenomena, it is essential to take into account the behavior of low- and high-shear rate blood behavior. With the choice of appropriate parameters corresponding to the experimental results for each non-Newtonian model, the dependence of viscosity on shear rate can be properly taken into account. There are many constitutive equations to represent the purely viscous properties of blood. In general, these models are divided into categories called Newtonian and generalized Newtonian (purely viscous). Among these, the most widely used to describe the variation of viscosity with shear rate are the power law model and the models of Casson-Carreau and Carreau-Yasuda (Shibeshi and Collins, 2005; Boyd et al., 2007; Morbiducci et al., 2011; Razavi et al., 2011).

It is accepted in the literature that generalized Newtonian models tend to increase the predicted value of WSS (Cho and Kensey, 1991; Baaijens et al., 1993). Works cited in (Py, 2002) and (Amblard and Bou-Saïd, 2004) have brought together different values of WSS calculated at the same shear rate and Reynolds number for different laws. The authors observed a very large disparity among the calculated values (Table 1). The lack of experimental validation data makes the predictions of these models very uncertain.

Table 1
Analytically determined wall stress for various generalized Newtonian models (Amblard and Bou-Saïd, 2004).

Name of law	Wall stress (Pa)
Bingham	0.405
Casson	0.015
Ostwald de Waele	0.697
Sisko	4

Moreover, none of these models takes into account the elasticity nor the thixotropy of blood. Therefore, this type of law may be insufficient to characterize the overall blood flow. The improvement proposed here reconciles the microstructural analysis of blood with lattice theory (Amblard and Bou-Saïd, 2004). It allows for a wider consideration of the rheological details of blood, in particulary the slip effects between the plasma and suspended globules. In this study, we choose to model the flow of blood in the aorta by a rheological model derived from this network theory: the model of Phan-Thien and Tanner. Its appropriate use for hemodynamic was studied by (Amblard and Bou-Saïd, 2004) but not validated with any clinical data. A slight modification to the model of Phan-Thien and Tanner permits taking the shear thinning effect of viscosity into account. The assumptions of this model, linked to the creation and destruction of microstructural bonds, appear to be representative of the observed phenomena.

3. Materials and methods

3.1. Fluxes measured by MRI in 2D and 4D

The dynamic flux measurements by MRI in 2D and 4D were performed on a healthy volunteer. All MR images were obtained on a 1.5 Tesla (T) Siemens Aera scanner (Erlangen Germany) using a thoracic coil placed on the chest. First, through-plane blood flow velocities were measured using a 2D phase contrast sequence (PC-MRV) with the following parameters: velocity encoding = 150 cm/s, TR/TE = 60.1/3.89 ms, FOV = 30 cm $\times$ 20 cm, slice thickness = 5.5 mm, voxel size = 1.6 mm $\times$ 1.6 mm. 30 time points were acquired through the cardiac cycle. Measurements were performed perpendicular to the supra aortic trunks and perpendicular to the descending aorta at midthoracic levels (T7). Those vessels are considered with little movement compared to the ascending aorta, thus producing more reliable measurements. Average flows during the cardiac cycle were then calculated at these two levels and flow values for the ascending aorta were obtained as the sum of the flows of the descending aorta and the supra aortic trunks.

A 4D MRI was also performed on the same patient using an RF spoiled gradient echo pulse sequence and an oblique sagittal slab encompassing the thoracic aorta. Scans were performed with respiratory compensation, retrospective electrocardiographic (ECG) gating and the following imaging parameters: velocity encoding = 150 cm/s in the three directions, TR/TE = 39.8/2.6 ms, FOV = 35 cm $\times$ 25 cm, slice thickness = 2.2 mm, voxel size = 2.2 mm $\times$ 2.2 mm $\times$ 2.2 mm, number of slices = 30. Thirty time points were acquired through the cardiac cycle. From these data, the flow segmentation procedure as illustrated in Fig. 1, was carried out with an in-house software.

3.2. Configuring the MPTT rheological model

The Navier-Stokes equations are solved for a laminar and incompressible flow using the free access software *OpenFOAM*. The walls are considered to be rigid. As a first step, the solution is carried out in the transient mode and for a Newtonian fluid whose dynamic viscosity is $\eta = 0.0035$ Pa-s. In the second stage, the non-Newtonian MPTT model and the generalized Newtonian model of Carreau are used. The MPTT model was implanted in *OpenFOAM* using the *ViscoelasticFluidFoam* solver (Favero et al., 2010). The constitutive equation for this model is (Bird et al., 1980):

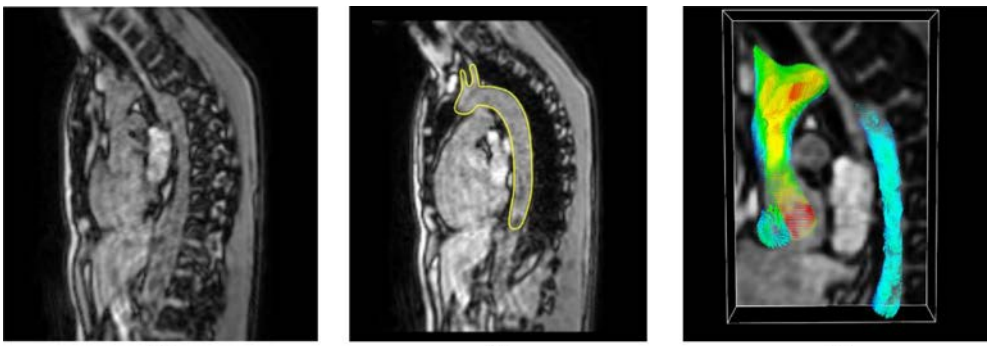

Fig. 1. Post-processing method of 4D MRI: (a) raw data, (b) segmentation of the volume of interest on all cuts at all phases of the cycle, (c) generation of velocity fields in the volume of interest with an in-house software.

$$\lambda_{i,0}\frac{D\tau_{ij}}{Dt} + \sigma_{ij}(tr\tau_{ij})\tau_{ij} = 2\eta_m D_{ij} \quad (1)$$

$$\sigma_{ij} = \exp\left(\in \frac{tr\tau_{ij}}{G_{i,0}}\right) \quad (2)$$

where τ_{ij} is the stress tensor, D_{ij} the deformation rate tensor, and η_m the viscosity given by the Carreau model:

$$\eta_m = \eta_p \frac{1 + \xi(2-\xi)\lambda^2\dot{\gamma}^2}{(1+\Gamma^2\dot{\gamma}^2)^{(1-n)/2}} \quad (3)$$

In the above equation, η_p is the red blood cell viscosity at low shear rate, ξ is the rate of slip between the globules and the plasma, λ is the characteristic time of the red blood cells, $\dot{\gamma}$ is the shear rate, Γ is a time parameter equal to $11.08 \times \lambda$, and n is the exponent of the power law. The numerical values are chosen to best represent the behavior of blood, and are adapted from (Amblard and Bou-Saïd, 2004) as summarized in Table 2.

3.3. Patient-specific model

In this study, the Digital Imaging and Communication (DICOM) images from MRI were processed with Simpleware ScanIP v7.0 2000-2014© commercial software. A geometric model of the aorta has been meshed with polyhedral elements generated with the commercial *Star-CCM +*© software. A mesh sensitivity study was carried out on the model based on the maximum numerical values of shear stress along the aorta. The study showed that a mesh with elements of about 0.3 mm^3 was adequate, or 478,000 elements in the model - 0.24% difference on the shear value from a 2,000,000 elements thin mesh.

3.4. Boundary conditions

A Poiseuille flow type velocity profile was applied to the entry of the thoracic aorta. This profile was adapted to the non-circular entry area using the method described by (Mynard & Nithiarasu, 2008). The parameters of the Windkessel model used were first assigned based on literature data (Vignon-Clementel et al., 2006; LaDisa et al., 2011; Xiao et al., 2013) for the three brachiocephalic vessels and the descending aorta of the numerical model. They were then manually adjusted on the basis of the dynamic imaging data. This variation of the parameters allows readjustment in relation to the patient's own data, thus providing patient-specific resistance and compliance values (Table 3).

Table 2
Parameter values for the MPTT model.

Symbol	Definition	Value
η_m	Blood dynamic viscosity at high shear rate	0.0035 Pa s
η_p	Blood dynamic viscosity at low shear rate	0.05 Pa s
ρ	Blood density	1060 kg m^{-3}
λ	Characteristic time of red blood cells	4.0×10^{-5} s
Γ	Time dimension parameter	$11.08 \times \lambda$ s
n	Power law exponent	0.8
ξ	Red cell/plasma slip rate	0.2

Table 3
3-Element Windkessel model parameters applied to the outputs of the fluid model and recalibrated with the 2D phase imaging data. R_1, R_2 and C denote, respectively, the hydraulic resistance of the ascending aorta, the hydraulic resistance of the vessel, and the compliance of the vessel.

	R_1 (m^{-1} s^{-1})	R_2 (10^6 m^{-1} s^{-1})	C (10^{-7} m s^2)
Brachiocephalic artery trunk	52,500	0.8337	8.6334
Left carotid artery	147,000	2.3203	3.1003
Left subclavian artery	71,985	1.2135	5.9511
Descending aorta	15,443	0.2603	0.2774

3.5. Numerical simulation parameters

After a sensitivity study, the time step for numerical computation of the non-Newtonian model was chosen as $\Delta t = 1 \times 10^{-5}$ s, based on the characteristic time of red blood cells $\lambda = 4.0 \times 10^{-5}$ s. This time step is much lower than that of the Newtonian case where $\Delta t = 1 \times 10^{-3}$ s. The viscoelastic properties of the fluid require a relatively small time step to capture the desired effects, as a function of the imposed boundary conditions. Convergence is usually reached after five cardiac cycles.

4. Results

4.1. Influence of the red cell viscosity η_p

The sensitivity of the MPTT model to the variation of certain rheological parameters is studied in this section. Our choice focused on the viscosity of red blood cells η_p, based on the observations of (Amblard et al., 2009). Variation in this parameter from case to case helps to represent the diversity of patients. Three different viscosity values were studied to estimate their influence on flow during the cardiac cycle. These values (η_p = 0.1, 0.05 and 0.01 Pa s) correspond to two normal adults and an afibrogenaemia patient respectively (Dintenfass, 1965).

Using Eq. (3), we calculated the equivalent viscosity η_m resulting from the different values of red blood cell viscosities at low and high shear rates (Table 4). We calculated numerical values of shear

rate $\dot{\gamma}$ in the case of different velocities v = 0.05–0.8 m/s, representing low and high shear rates respectively and an aorta mean radius R = 0.015 m:

$$\dot{\gamma} = \frac{v}{2R} \tag{4}$$

The difference observed between high and low shear rate equivalent viscosities for each η_p is 23% (Table 4).

Fig. 3 shows the velocity profiles on several cross-sections along the aorta during an instant of flow rate decrease (t = 0.19 s), and another during the diastole phase (t = 0.42 s), and at several viscosities. It is noted that a high value of η_p insures relatively homogeneous velocity profiles regardless of the instant of time observed. During the systolic phase, the influence of viscosity is less relative to diastolic conditions. When η_p = 0.1 Pa s, the blood is more viscous and therefore more difficult to shear, even if the helical shape of the flow is still visible, due to the particular geometry of the aortic arch. When η_p = 0.01 Pa s, the mean viscosity approaches the viscosity of the blood with the assumption of a Newtonian fluid in which η = 0.003–0.006 Pa s. Velocity profiles that approximate those noted in the Newtonian case are then observed. Therefore, the viscosity η_p = 0.01 Pa s appears to represent a minimum threshold beyond which the shear thinning character of the blood appears in the flow.

Fig. 4 shows the WSS distribution at t = 0.12 s and t = 0.42 s, systolic and diastolic, respectively, with several viscosities. The shear stress τ_w corresponds to the frictional forces exerted by the blood flow onto the vascular wall. For a Newtonian fluid, this stress depends on the fluid dynamic viscosity μ and the longitudinal velocity gradient estimated at the wall surface (i.e., y = 0):

$$\tau_w = \mu\left(\frac{\partial u}{\partial y}\right)_{y=0} \tag{5}$$

The observations are made here are similar to previous cases when studying the viscosity effect on velocity distribution. A decrease of the fluid viscosity leads to a decrease of the shear stress which is in accordance with relation (4) (Fig. 4). In addition, wall shear stress values are much higher during systole (Fig. 4) because of the significant acceleration of flow at the cardiac cycle. The wall shear stress along the aortic arch contour is illustrated in Fig. 5 for four cuts A, B, C and D located in Fig. 3. As expected, a higher viscosity value provides a higher wall shear stress value, whatever the location in the aorta. Furthermore when considering cuts A, B and C, the shear stress varies significantly over the surface. This highlights the highly inhomogeneous flow in these regions. This variation is not observed for section D located on the descending aorta, and corresponds to a region where the velocities are no longer influenced by the aortic arch geometry.

4.2. Comparison with the generalized Newtonian model of Carreau

The Carreau model is widely used in the literature for the blood flow modeling (O'Callaghan et al., 2006; Biasetti et al., 2011; Toloui et al., 2012). It is a generalized Newtonian model exhibiting plateaus of viscosity at both low and high shear rates. The variation of the viscosity function in the MPTT model is given by the Carreau

Table 4
Equivalent viscosities η_m for the MPTT model at different shear rates for three different red blood cell viscosities.

η_p = 0.1 Pa s		η_p = 0.05 Pa s		η_p = 0.01 Pa s	
v (m/s)	η_m (Pa s)	v (m/s)	η_m (Pa s)	v (m/s)	η_m (Pa s)
0.05	0.0870	0.05	0.0435	0.05	0.0087
0.8	0.0708	0.8	0.0354	0.8	0.0071

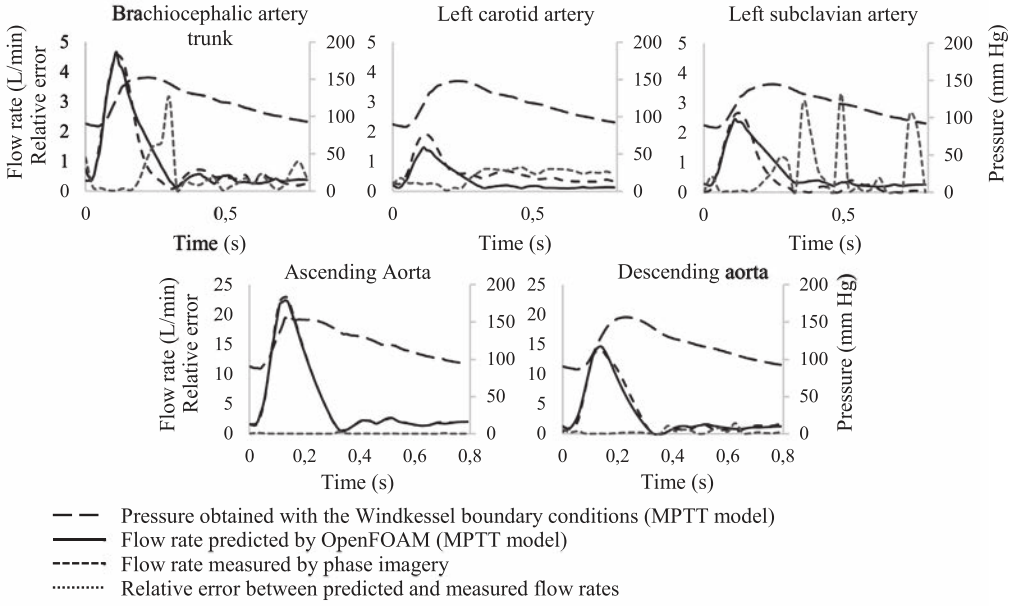

Fig. 2. Time evolution of pressure and flow rate at different boundary conditions during a cardiac cycle. The comparison between the flow rates obtained from dynamic imagery (dotted line) and the measured flows with the MPTT model in *OpenFOAM* (blue line) shows the recalibration of the Windkessel model parameters. Relative error shows a good accuracy for the ascending and descending aorta.

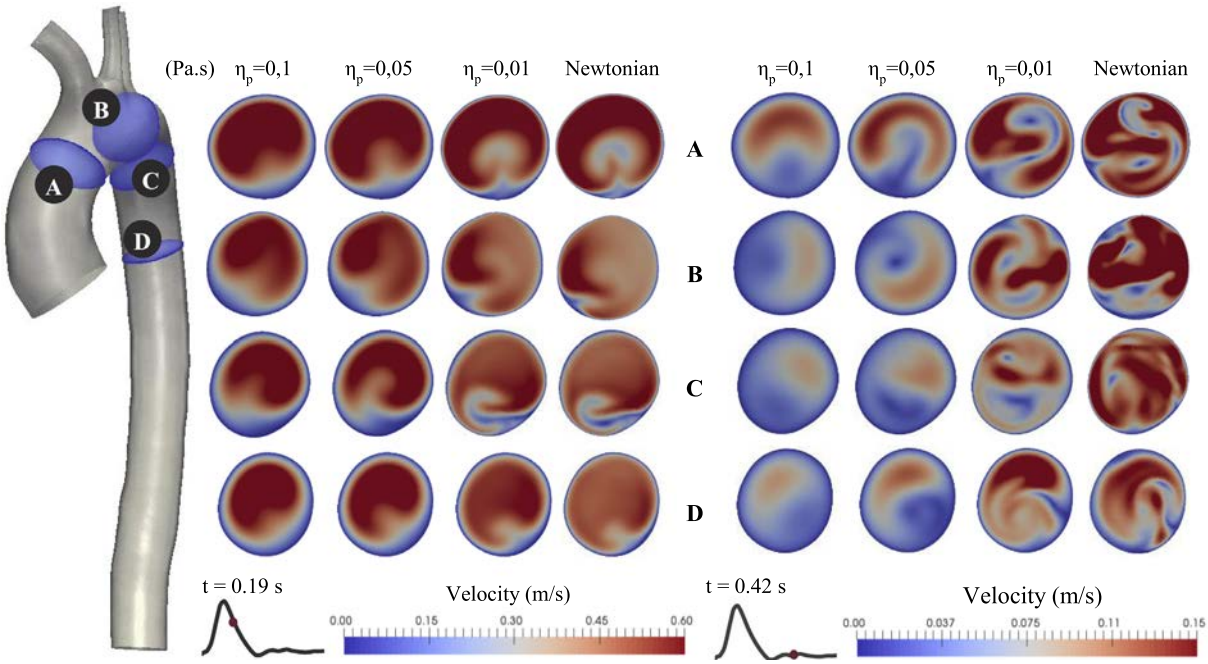

Fig. 3. Velocity distributions on several cross-sections, at times t = 0.19 s and t = 0.42 s, with several viscosities for the MPTT model and for a Newtonian fluid.

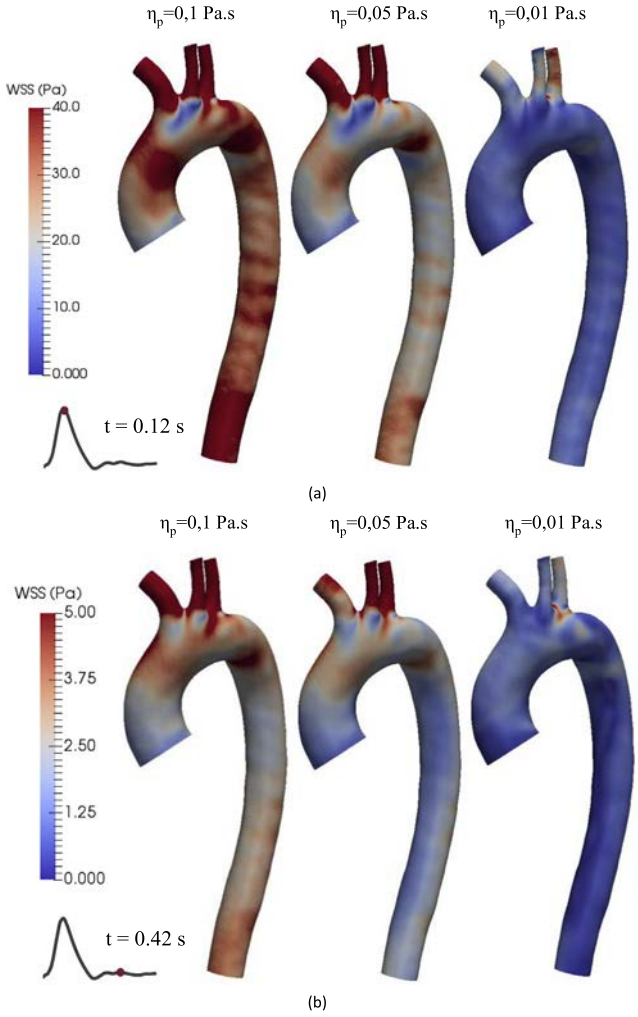

Fig. 4. Wall Shear Stress (WSS) distribution on aorta surface (a) at t = 0.12 s and (b) at t = 0.42 s, and several viscosities for the MPTT model.

model, thus a comparison of numerical results with these two models is interesting. This model has a viscosity that varies according to the following equation:

$$\eta = \eta_\infty + \frac{\eta_0 - \eta_\infty}{(1 + (k\dot{\gamma}))^{2/(n-1)}} \tag{6}$$

where $\dot{\gamma}$ is the shear rate, η_0 = 0.00345 Pa s is the dynamic viscosity of blood at high shear rate, η_∞ = 0.056 Pa s is the dynamic viscosity of blood at low shear rate and, n = 0.3568 is the power law exponent parameter (Razavi et al., 2011).

One observes that using the Carreau model or the Newtonian model with μ = 0.0035 Pa s yields similar velocity distributions during both the systolic (t = 0.19 s) and the diastolic (t = 0.42 s) regimes (Fig. 6). The shear thinning character of the blood is thus only slightly exhibited by the Carreau model. The shear stresses become very low and correspond closely to the velocity distributions obtained by the Newtonian model.

4.3. Comparison with 4D MRI data

The comparison between the flows obtained by dynamic imaging and the calculated flows with the MPTT model (Fig. 2) shows a good agreement for each output.

We observe a high degree of accuracy when comparing experimental with numerical results for the ascending and descending aorta, while differences are observed for the three brachiocephalic vessels mainly due to the Windkessel boundary conditions. These vessels are however far from the area of interest, thus those differences will not influence the flow into the aorta.

The comparison between the MPTT model and the *in vivo* data of dynamic imaging is portrayed in Fig. 6. The MPTT model (η_p = 0.05 Pa s) shows more similarity to the 4D MRI data during the systolic and diastolic phases than the Newtonian model or the generalized Newtonian Carreau model, which confirms our interest in using both a rheological model as complex as the MPTT, and using a red blood cell viscosity close to 0.05 Pa s.

The rigid wall model used for these simulations gives initial estimates of flux compared with 4D dynamic imaging. The param-

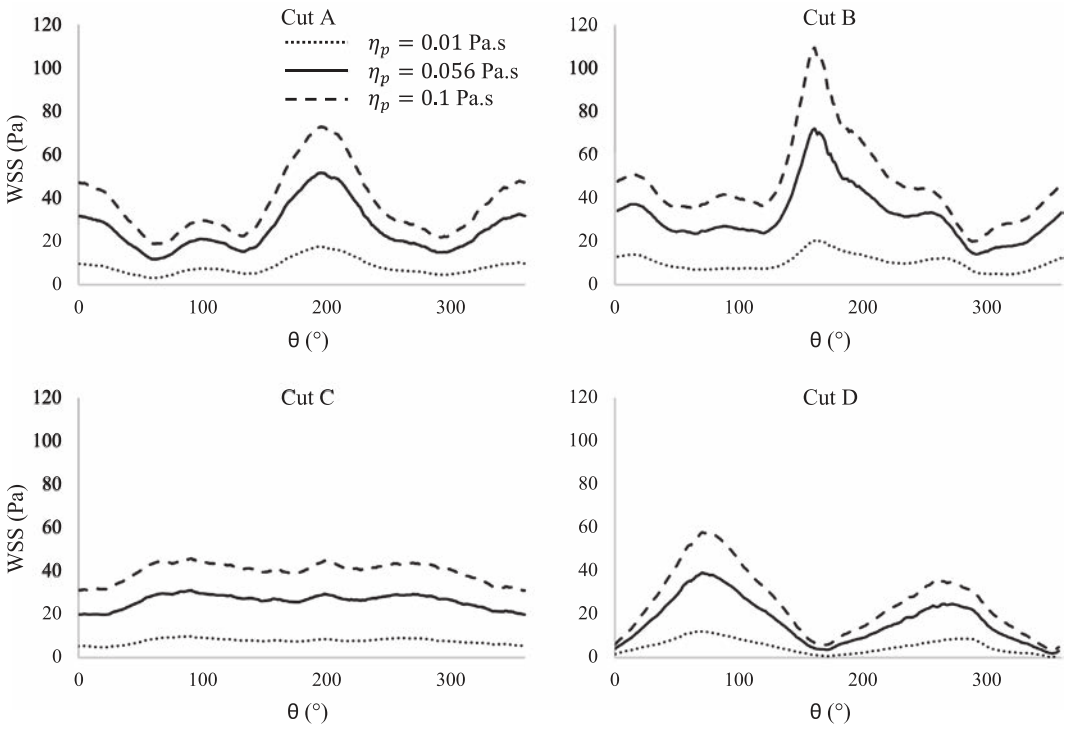

Fig. 5. Influence of viscosity on the shear stress, at t = 0.12 s (systolic peak), along the contour of the cuts according to several viscosities, for the model MPTT model, η_p = 0.1, 0.05, and 0.01 Pa s. See Fig. 3 for location of the cuts.

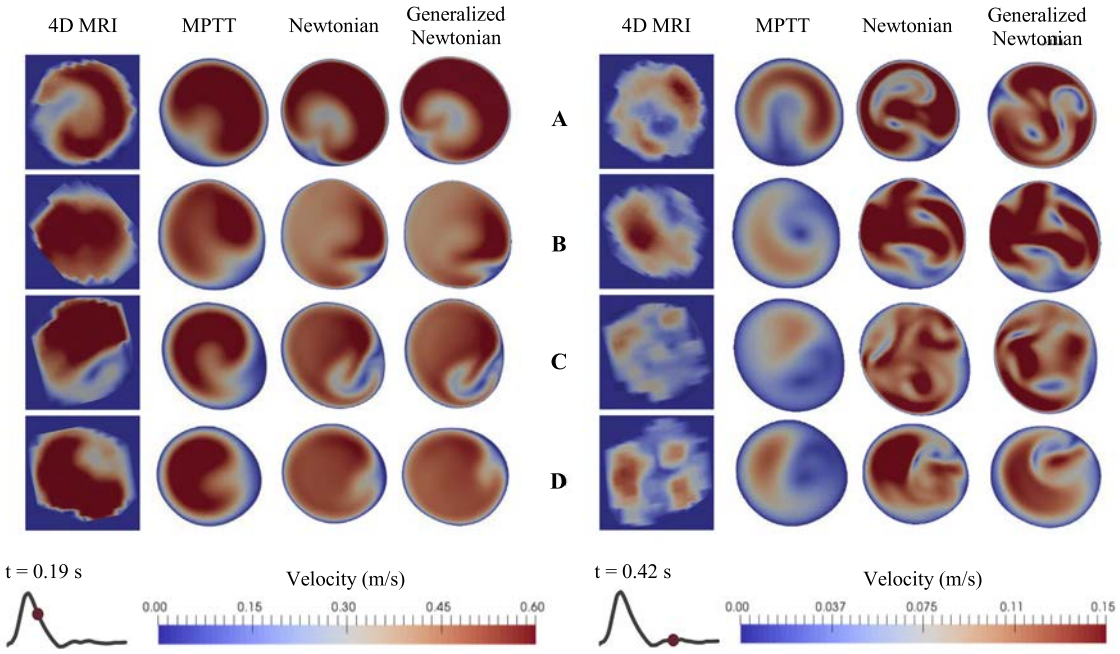

Fig. 6. Comparison of velocity distributions on several cross-sections (locations as shown in Fig. 3), at t = 0.19 s and t = 0.42 s between the dynamic MRI data, and the MPTT, Newtonian, and generalized Newtonian models.

eters of these models influence the results of numerical calculations. The experimental data permit readjustment of the numerical values of these parameters and thus benefit is obtained from a coherent model.

5. Discussion

In the aorta, the flow is normally thought to be laminar (Antiga & Steinman, 2009) but is considered to be in transition from laminar to turbulent at the systolic peak only. However, in our simulations, we considered the flow to be strictly laminar throughout the cardiac cycle which can have an impact on the WSS evaluation.

We used dynamic imaging to see if the numerical approach is capable of predicting pressure and velocity fields. However, a number of factors may compromise the accuracy of this method. These include limitations on spatial and temporal resolution that result in incomplete results in certain areas. Other factors, such as imperfections related to magnetic field disturbances, may also challenge

the precision. This is particularly critical for the *in vivo* determination of velocity-derived quantities such as shear stresses in complex flow regions (Boussel et al., 2009), hence the need for a precise rheological model.

The boundary conditions of Windkessel have allowed us to take into account the hydraulic resistance of the remainder of the arterial network that is not directly modeled (i.e., outside the major arteries) and the compliance of the arteries. This lumped parameter model makes it possible to vary the output pressure of the branches throughout the cardiac cycle and thus to respect the physiological variation of flow with the pressure. This constitutes an acceptable compromise between model complexity and physiological reality.

The parabolic inlet profile is suitable for fully developed flows in circular conduits. An alternative is to use the Womersley profile (Womersley, 1955; Uchida, 1956), which is well adapted to the oscillatory regime of the cardiac cycle. Although the Womersley profile describes flow in the arteries, it does not fit that well with the ejection profile of blood from the heart. Poiseuille flow is widely used in the literature (Reymond et al., 2009; Wen et al., 2010), its popularity mainly being based on the fact that it is easy to use and understand. In this study, the introduction of an input profile from 4D MRI data showed a small influence on the flow profiles in the aortic arch and the descending aorta. However, a more detailed study at the exit of the heart, and in the ascending thoracic aorta, would require the use of a patient-specific velocity profile (Gallo et al., 2012; Morbiducci et al., 2013). In this complex situation, we used a temporally varying parabolic flow profile, which is more stable numerically.

The use of a rigid wall model remains debatable for the validation of the rheological model used, thus the need for simulations of fluid-structure interactions (FSI) to approximate physiological conditions. Indeed, the ascending aorta and the aortic arch are the most deformed under the effect of cardiac pressure variation. Their diameter increases by about 10% (Morrison et al., 2009). The problem of FSI is widely studied in the literature (Molony et al., 2009), but its great numerical complexity requires additional simplifying hypotheses on the mechanical properties of arterial tissue and the boundary conditions on the structure. In the literature, modeling of the surrounding tissues of the aorta can be carried out by springs representing tethering the solid structure to the spine (Mouktadiri et al., 2013). In other studies, a viscoelastic mathematical model is applied to the entire aortic surface (Moireau et al., 2012; Reymond et al., 2013). However, these models tend to generate many numerical instabilities.

6. Conclusions

The present study allows hemodynamic behavior to be simulated in a healthy thoracic aorta for a specific patient. One of the primary ambitions and objectives in hemodynamic modeling is to best represent the particularities of the flows. This cannot be done without a relevant and appropriate rheological model of blood in complex locations of human anatomy.

The pulsatile character of the flow affects the rheological character of blood and therefore requires a representative constitutive model for the best assessment of blood pressure on the arterial wall and velocity fields. The rigid wall model used for these simulations gives initial estimates of flux compared with data from dynamic imaging. The problem of capturing all the relevant physics in a reasonable computational time to provide accurate results to surgeons is still a matter of ongoing research.

The numerical results obtained are encouraging and show the effectiveness of the MPTT model to describe the hemodynamics relative to the generalized Newtonian models. Data from 4D MRI are of paramount importance in validating hemodynamic simulation. The correct determination of the pressure and velocity fields on the one hand constitutes an interesting platform for a correct analysis of the placement of aortic prostheses, and on the other hand serves as a starting point for a mechano-transduction study of the genesis of arterial pathologies.

Exponential improvement in medical imaging techniques makes it increasingly possible to reconcile the needs of clinicians with the tools of engineers and scientists. *In-vivo* data, such as patient real-time flux, obtained by clinicians set the stage for great advances in numerical modeling.

Conflict of interest

All authors declare that they have no conflicts of interest.

Statement of ethics

All the tests and procedures have been approved by the French ethical committee and were performed in subjects who gave informed consent.

Acknowledgement

The authors thank the Institut Carnot de Lyon I@L for the funding of this research project.

References

Amblard, A., Bou-Saïd, B., 2004. Modelling the blood flow in an aorta; the MPTT and Modified MPTT models. Tribol. Interface Eng. Ser. 48, 381–387.
Amblard, A., Walter-Le Berre, H., Bou-Saïd, B., Brunet, M., 2009. Analysis of type I endoleaks in a stented abdominal aortic aneurysm. Med. Eng. Phys. 31, 27–33.
Antiga, L., Steinman, D.A., 2009. Rethinking turbulence in blood. Biorheology 46 (2), 77–81.
Baaijens, J.P.W., Van Steenhoven, A.A., Janssen, J.D., 1993. Numerical analysis of steady generalized Newtonian blood flow in a 2D model of the carotid artery bifurcation. Biorheology-Oxford 30, 63.
Biasetti, J., Hussain, F., Gasser, T.C., 2011. Blood flow and coherent vortices in the normal and aneurysmatic aortas: a fluid dynamical approach to intra-luminal thrombus formation. J. Roy. Soc. Interface, p. rsif20110041.
Bird, R.B., Dotson, P.J., Johnson, N.L., 1980. Polymer solution rheology based on a finitely extensible bead-spring chain model. J. Nonnewton. Fluid Mech. 7 (2–3), 213–235.
Boussel, L. et al., 2009. Phase-contrast magnetic resonance imaging measurements in intracranial aneurysms in vivo of flow patterns, velocity fields, and wall shear stress: comparison with computational fluid dynamics. Magn. Reson. Med. 61, 409–417.
Boyd, J., Buick, J.M., Green, S., 2007. Analysis of the Casson and Carreau-Yasuda non-Newtonian blood models in steady and oscillatory flows using the lattice Boltzmann method. Phys. Fluids 19, 093103.
Cho, Y.I., Kensey, K.R., 1991. Effects of the non-Newtonian viscosity of blood on flows in a diseased arterial vessel. Part 1: Steady flows. Biorheology 28, 241–262.
Dintenfass, L., 1965. Viscosity of the packed red and white blood cells. Exp. Mol. Pathol. 4 (6), 597–605.
Dwyer, H.A., Cheer, A.Y., Barakat, A.I., Rutaganira, T., 2002. Unsteady and three-dimensional simulation of blood flow in the human aortic arch. Trans. ASME 124, 378–387.
Favero, J.L., Secchi, A.R., Cardozo, N.S.M., Jasak, H., 2010. Viscoelastic flow analysis using the software OpenFOAM and differential constitutive equations. J. Non-Newtonian Fluid Mech. 165, 1625–1636.
Figueroa, C.A. et al., 2009. Effect of curvature on displacement forces acting on aortic endografts: a 3-dimensional computational analysis. J. Endovascular Therapy 16, 284–294.
Gallo, D. et al., 2012. On the Use of in vivo measured flow rates as boundary conditions for image-based hemodynamic models of the human aorta. Implications for indicators of abnormal flow. Ann. Biomed. Eng. 40, 729–741.
Gallo, D. et al., 2016. A patient-specific follow up study of the impact of thoracic endovascular repair (TEVAR) on aortic anatomy and on post-operative hemodynamics. Comput. Fluids 141, 54–61.
Hope, M.D. et al., 2010. Bicuspid aortic valve: four-dimensional MR evaluation of ascending aortic systolic flow patterns. Radiology 255, 53–61.
LaDisa, J.F. et al., 2011. Computational simulations for aortic coarctation: representative results from a sampling of patients. J. Biomech. Eng. 133 (9), pp. 091008-091008-9.

Liu, X. et al., 2009. A numerical study on the flow of blood and the transport of LDL in the human aorta: the physiological significance of the helical flow in the aortic arch. Am. J. Physiol.-Heart Circulatory Physiol. 297, H163–H170.
Löhner, R. et al., 2003. Applications of patient-specific CFD in medicine and life sciences. Int. J. Numer. Methods Fluids 43, 637–650.
Markl, M. et al., 2010. Estimation of global aortic pulse wave velocity by flow-sensitive 4D MRI. Mag. Reson. Med. 63, 1575–1582.
Millon, A. et al., 2014. A new carotid 3D MRI sequence for stenosis measurement and plaque characterization at the same time. Eur. J. Vasc. Endovasc. Surg. 48, 342.
Moireau, P. et al., 2012. External tissue support and fluid–structure simulation in blood flows. Biomech. Model. Mechanobiol. 11, 1–18.
Molony, D.S. et al., 2009. Fluid-structure interaction of a patient-specific abdominal aortic aneurysm treated with an endovascular stent-graft. Biomed. Eng. Online 8, 1.
Moore, J.A., Steinman, D.A., Holdsworth, D.W., Ethier, C.R., 1999. Accuracy of computational hemodynamics in complex arterial geometries reconstructed from magnetic resonance imaging. Ann. Biomed. Eng. 27, 32–41.
Morbiducci, U. et al., 2011. On the importance of blood rheology for bulk flow in hemodynamic models of the carotid bifurcation. J. Biomech. 44, 2427–2438.
Morbiducci, U. et al., 2013. Inflow boundary conditions for image-based computational hemodynamics: impact of idealized versus measured velocity profiles in the human aorta. J. Biomech. 46, 102–109.
Morris, L. et al., 2005. 3-D numerical simulation of blood flow through models of the human aorta. J. Biomech. Eng. 127, 767–775.
Morrison, T.M., Choi, G., Zarins, C.K., Taylor, C.A., 2009. Circumferential and longitudinal cyclic strain of the human thoracic aorta: age-related changes. J. Vascular Surgery, #apr# 49 (4), 1029–1036.
Mouktadiri, G., Bou-Saïd, B., Walter-Le-Berre, H., 2013. Aortic endovascular repair modeling using the finite element method. J. Biomed. Sci. Eng. 6, 917–927.
Mynard, J.P., Nithiarasu, P., 2008. A 1D arterial blood flow model incorporating ventricular pressure, aortic valve and regional coronary flow using the locally conservative Galerkin (LCG) method. Commun. Numer. Methods Eng. 24, 367–417.
Nayak, K.S. et al., 2015. Cardiovascular magnetic resonance phase contrast imaging. J. Cardiovasc. Magn. Reson. 17, 71.
O'Callaghan, S., Walsh, M., McGloughlin, T., 2006. Numerical modelling of Newtonian and non-Newtonian representation of blood in a distal end-to-side vascular bypass graft anastomosis. Med. Eng. Phys. 28, 70–74.
Pedersen, E.M. et al., 1999. Distribution of early atherosclerotic lesions in the human abdominal aorta correlates with wall shear stresses measured in vivo. Eur. J. Vascular Endovascular Surgery 18, 328–333.
Pedersen, E.M., Sung, H.-W., Burlson, A.C., Yoganathan, A.P., 1993. Two-dimensional velocity measurements in a pulsatile flow model of the normal abdominal aorta simulating different hemodynamic conditions. J. Biomech. 26, 1237–1247.
Py, C., 2002. Modélisation de l'écoulement sanguin: rapport de Master spécialité Mécanique, Lyon: s.n.
Rayz, V.L. et al., 2015. Computational modeling of flow-altering surgeries in basilar aneurysms. Ann. Biomed. Eng. 43, 1210–1222.
Rayz, V.L. et al., 2008. Numerical simulations of flow in cerebral aneurysms: comparison of CFD results and in vivo MRI measurements. J. Biomech. Eng. 130, 051011.
Rayz, V.L. et al., 2010. Flow residence time and regions of intraluminal thrombus deposition in intracranial aneurysms. Ann. Biomed. Eng. 38, 3058–3069.
Razavi, A., Shirani, E., Sadeghi, M.R., 2011. Numerical simulation of blood pulsatile flow in a stenosed carotid artery using different rheological models. J. Biomech. 44, 2021–2030.
Reymond, P. et al., 2013. Physiological simulation of blood flow in the aorta: comparison of hemodynamic indices as predicted by 3-D FSI, 3-D rigid wall and 1-D models. Med. Eng. Phys. 35, 784–791.
Reymond, P. et al., 2009. Validation of a one-dimensional model of the systemic arterial tree. Am. J. Physiol. Heart Circulatory Physiol. 297, H208–H222.
Shibeshi, S.S., Collins, W.E., 2005. The rheology of blood flow in a branched arterial system. Appl. Rheol. (Lappersdorf, Germany: Online) 15, 398.
Sigovan, M. et al., 2015. Extended 3D approach for quantification of abnormal ascending aortic flow. Magn. Reson. Imaging 33, 695–700.
Sigovan, M., Hope, M.D., Dyverfeldt, P., Saloner, D., 2011. Comparison of four-dimensional flow parameters for quantification of flow eccentricity in the ascending aorta. J. Magn. Reson. Imaging 34, 1226–1230.
Stankovic, Z. et al., 2014. 4D flow imaging with MRI. Cardiovasc. Diagnosis Therapy 4.
Taylor, C.A., Hughes, T.J.R., Zarins, C.K., 1998. Finite element modeling of blood flow in arteries. Comput. Methods Appl. Mech. Eng. 158, 155–196.
Toloui, M., Firoozabadi, B., Saidi, M.S., 2012. A numerical study of the effects of blood rheology and vessel deformability on the hemodynamics of carotid bifurcation. Scientia Iranica 19, 119–126.
Uchida, S., 1956. The pulsating viscous flow superposed on the steady laminar motion of incompressible fluid in a circular pipe. Zeitschrift f{\"u}r angewandte Mathematik und Physik ZAMP 7, 403–422.
Vignon-Clementel, I.E., Figueroa, C.A., E. Jansen, K., Taylor, C.A., 2006. Outflow boundary conditions for three-dimensional finite element modeling of blood flow and pressure in arteries. Comput. Methods Appl. Mech. Eng. 195 (29), 3776–3796.
Wen, C., Yang, A., Tseng, L., Chai, J., 2010. Investigation of pulsatile flowfield in healthy thoracic aorta models. Ann. Biomed. Eng. 38, 391–402.
Womersley, J.R., 1955. Method for the calculation of velocity, rate of flow and viscous drag in arteries when the pressure gradient is known. J. Physiol. 127, 553.
Xiao, N., Humphrey, J.D., Figueroa, C.A., 2013. Multi-scale computational model of three-dimensional hemodynamics within a deformable full-body arterial network. J. Comput. Phys. 244, 22–40.